Time-resolved second harmonic generation with single-shot phase sensitivity

Alexandra L. Tyson, David A. Woods, and *Jan R. R. Verlet**

Abstract

A time-resolved, phase-sensitive second harmonic generation (SHG) method to probe the excited state dynamics of interfacial species is presented. It is based on an interference measurement between the SHG from a sample and a local oscillator (LO) generated at a reference surface in which an entire interference pattern is recorded in a single shot by using a spatially varying phase unit comprised of a pair of wedges that sandwich the reference sample. In combination with 30 kHz modulation of the experiment, shot-to-shot pump-probe measurements are presented. The technique is characterised by measuring the time-resolved change in the amplitude and phase of the interference pattern due to the excited state dynamics of the dye malachite green (MG) at the air/water interface. The key attributes of the technique are its excellent phase stability and sensitivity, and relatively short data acquisition times.

* j.r.r.verlet@durham.ac.uk

I. Introduction

Second harmonic generation (SHG) and sum-frequency generation (SFG) are non-linear optical processes that occur when high intensity light interacts with materials that are non-centrosymmetric. While extensively used in the frequency conversion of lasers using non-centrosymmetric crystals, SHG and SFG have also found important applications in probing surfaces between two centrosymmetric media, where the inversion symmetry is necessarily broken.[1–7] Although very surface-specific, SHG and SFG inherently produces weak signals because only a small interfacial region where inversion-symmetry is broken contributes to the macroscopic signal. For SHG, the measured signal is proportional the squared second-order non-linear susceptibility, $I_{SHG} \alpha |\chi^{(2)}|^2$, with $\chi^{(2)} = N_S\langle\beta\rangle$, where N_S is the number of molecules per unit area and $\langle\beta\rangle$ the orientationally averaged hyperpolarizability. Therefore, the directly measured signal $I_{SHG} \propto N_S^2$ and most experiments (especially SFG) have focussed on interfaces where N_S is very large such as pure water or surfactant solutions. Adsorbates can be probed and resonance enhancement of the SHG signal by the adsorbate can greatly increase the signals. This has enabled detailed studies of the spectroscopy,[1,8–16] orientation,[17–20] and dynamics[21–29] of molecular adsorbates at interfaces. Photoinitiated dynamics of such adsorbates are particularly interesting as an important case between fully solvated and isolated species. However, SHG/SFG experiments are particularly difficult because only a small subset of adsorbates is excited by a pump pulse, so that a probe produces small changes in an already weak SHG/SFG signal. Moreover, the measured SHG/SFG signal scales as N_S^n, with n is somewhere between 1 and 2 depending on the relative contributions between resonant and non-resonant parts of the total second-order non-linear susceptibility. While the assumption is often made that the resonant part dominates (so that $n \rightarrow 2$), this can fail for adsorbates with weak nonlinear responses or at low concentration (*e.g.* for excited states).[30] To overcome the unfavourable n-power dependence

on N_S, second order-nonlinear spectroscopy is often performed as a phase-sensitive measurement.[5,17,30–32] In this, the generated second harmonic electric field, $\mathbf{E}_{SHG}$, is interfered with an SHG field produced by a reference surface; the local oscillator, $\mathbf{E}_{LO}$. The total measured signal is then $S_{SHG} = \mathbf{E}_{SHG}^2 + \mathbf{E}_{LO}^2 + 2\mathbf{E}_{SHG}\mathbf{E}_{LO}\sin(\phi)$, where ϕ is the phase between $\mathbf{E}_{SHG}$ and $\mathbf{E}_{LO}$. By extracting only the interference term, $2\mathbf{E}_{SHG}\mathbf{E}_{LO}\sin(\phi)$, the measured signal becomes linearly dependent on N_S.

In a previous paper,[30] we detailed a phase-sensitive time-resolved SHG technique in which the phase between $\mathbf{E}_{SHG}$ and $\mathbf{E}_{LO}$ was changed manually by incrementally varying the distance between the sample and reference surface. A full interference fringe pattern was then constructed by measuring several points of constructive and destructive interference between $\mathbf{E}_{SHG}$ and $\mathbf{E}_{LO}$. The interference term was extracted by means of a lock-in measurement, in which a window was introduced into the beam path every second shot, leading to a temporal shift that removed the interference and thus allowed subtraction of the large nonlinear offset ($\mathbf{E}_{SHG}^2 + \mathbf{E}_{LO}^2$). The key benefit of the method was excellent phase stability over many hours of operation and high sensitivity. This enabled us to probe the charge-transfer-to-solvent dynamics of photoexcited iodide at the water/air interface.[33] However, the method proved to be sensitive to alignment, and suffered from long acquisition times because of the requirement to measure dynamics at various phase positions. The long acquisition times made the experiment susceptible to long-term laser power and alignment drifts. In the present paper, we present an improved methodology that enhances sensitivity, dramatically reduces acquisition times and retains the excellent phase stability.

II. Methodology

The new interference set up is inspired by a technique described by Stolle *et al.*,[34] where a pair of glass wedges are moved to generate a variable thickness of glass between a sample

and reference and thus vary the phase delay between the two signals. Instead, here, the reference surface is placed *between* a pair of CaF_2 wedges as shown in Figure 1(a) to create a spatially varying phase unit. While the fundamental beam (red) passes through both wedges and has a constant pulse front across the spatial profile of the beam, the generated LO (shown in blue) only propagates through one wedge, resulting in a continuously varying phase (and group) delay across the spatial beam profile. If both beams are directed onto a sample, the fundamental generates $\mathbf{E}_{SHG}$ with a flat pulse front, which will interfere with $\mathbf{E}_{LO}$. As the latter has a tilted spatial pulse front, the interference of $\mathbf{E}_{SHG}$ and $\mathbf{E}_{LO}$ will vary across the spatial profile of the beam. Consequently, the entire interference fringe pattern can be imaged on a position sensitive detector (CCD) with no moving components. In this manner, the need to scan the phase in our previous implementation is removed.

The cartoon in Figure 1(b) shows the $\mathbf{E}_{SHG}$ and $\mathbf{E}_{LO}$ as a function of both position and time with the interference pattern superimposed along the beam profile. The measured (projected) signal is also shown. A Fourier transform of the interference pattern provides both real (x) and imaginary (y) parts that can be used to extract the interference amplitude, A, and phase, Φ, using the equations:

$$A = (x^2 + y^2)^{½}, \tag{1}$$

and

$$\Phi = \tan^{-1}(y/x). \tag{2}$$

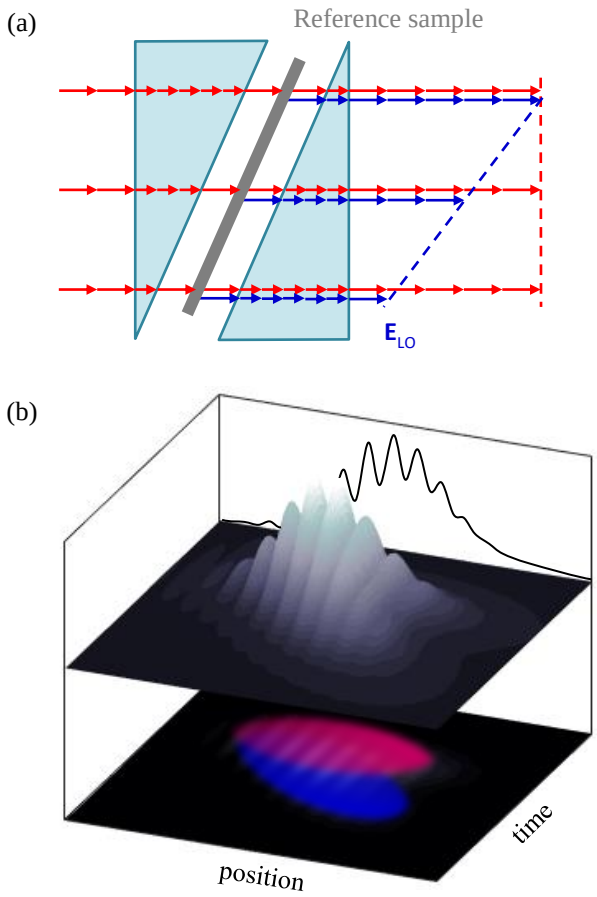

FIG 1. (a) Schematic of spatially varying phase unit. A reference surface, where $\mathbf{E}_{LO}$ is produced, is placed between two wedges. The arrows represent the position at varying times, with the dashed lines representing the pulse front of $\mathbf{E}_{LO}$ (blue) and the fundamental (pink). (b) A cartoon showing $\mathbf{E}_{SHG}$ (pink) and $\mathbf{E}_{LO}$ (blue) as a function of position and time. The interference pattern is superimposed across the beam's spatial profile. This is then projected (black line) onto a CCD sensor.

The fact that the entire interferogram is measured in a single shot has removed the need to perform a lock-in measurements to acquire the phase as was previously done. Consequently, the lock-in measurement can be applied to the pump-probe step of the experiment. Specifically, the pump is modulated to half the repetition rate of the laser to generate either a 'pump-probe' or 'probe-only', resulting in a shot-to-shot 'pump-off' reference. This approach is common in pump-probe experiments as it reduces excess noise. While straightforward to implement at low laser repetition rates using mechanical choppers, at repetition rates above a few kHz, excessive

jitter can be introduced.[35,36] Moreover, the requirement for a position sensitive detector places limits on the acquisition rates. For high-sensitivity CMOS or CCD cameras, the readout rates are typically slow in relation to commercially available laser systems (unlike single channel detection which is available with rates in the GHz regime).

To overcome the above limitation, some pump-probe experiments use a separate reference beam that is detected simultaneously with the signal beam on two separate detectors or on two separate regions of the same multichannel detector.[37–39] Here, we have adopted an approach using a Pockels cell and Wollaston prism to project both the 'pump-probe' signal and 'probe-only' background pulses onto different regions of the same 2D sensor (see Figure 2), allowing longer integration times without compromising the enhanced energy correlation of successive laser pulses and associated noise reduction.[35,36]

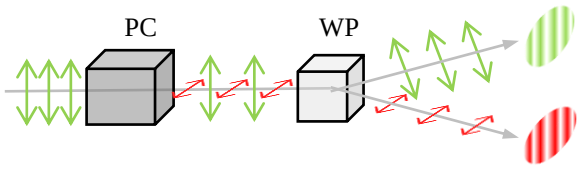

FIG 2. A schematic of the detection set up comprised of a Pockels cell (PC) and a Wollaston prism (WP), used to separate the pump-probe and probe-only signals before detection on the CCD.

III. Experimental

The experimental implementation of the above is shown schematically in Figure 3. Our main scientific interests are in ions at aqueous interfaces, and to demonstrate the methodology, we study the ambient water/air interface with malachite green (MG) as a cationic adsorbate that has previously been studied extensively.[28,30,40–43] All laser pulses were derived from a Yb:KGW laser system (Carbide, Light Conversion) providing 230 fs pulses with a 84 µJ pulse energy centred around 1028 nm with a repetition rate of 60 kHz. Around 30 µJ pulse^{-1} was

used to generate the fundamental probe beam from a commercial optical parametric amplifier (Orpheus, Light Conversion) at 800 nm. The fundamental (1.7 μJ pulse^{-1}) then propagated through a wedge pair (CaF_2, 10° angle, Crystran) which sandwiched a ~10 μm thin BBO crystal supported on a substrate (fused silica, 2 mm thick) that acted as the reference surface to produce $\mathbf{E}_{LO}$ (note that the substrate faces the first wedge). The collinearly propagating LO and fundamental beams were subsequently focused onto the sample surface using a concave mirror (f = 20 cm) at a ~70° angle of incidence to the water/air surface. The polarisation was controlled using a λ/2 plate prior to the wedge-pair and was set to be P-polarised in the present experiments.

The remaining 54 μJ pulse^{-1} from the main laser was used to generate the pump beam. The pump beam was first chopped at 30 kHz using a RTP crystal (Leysop) that switched polarisation of the 1028 nm light. A subsequent polarising beam splitter was used to reflect and dump alternate pulses from the 60 kHz train. The 1028 nm fundamental was frequency converted to the fourth harmonic in two consecutive BBO crystals, yielding 257 nm pulses and 1.3 μJ pulse^{-1} with <150 fs pulse duration. The pump was then focused by a concave mirror (f = 20 cm) onto the sample surface and overlapped spatially with the probe. The pump beam reflected from the surface was subsequently blocked. The delay between pump and probe pulses was controlled by a commercial motorised delay stage (Physik Instrumente).

After the SHG at the sample surface, the reflected fundamental, $\mathbf{E}_{SHG}$ and $\mathbf{E}_{LO}$ were re-collimated using a lens (f = 10 cm). The remaining fundamental was subsequently removed using filters and mirrors selective for the SHG wavelength (400 nm). The output polarisation was selected by a Glan-Taylor polarizer. In the present experiments, only the P output polarisation was selected so that the dipole-allowed PP polarization combination was probed.

The interfering $\mathbf{E}_{SHG}$ and $\mathbf{E}_{LO}$ then propagated through an ADP crystal (Leysop) that was switched at 30 kHz synchronised to the modulation of the pump pulse. The resulting S and

P polarised pulses (which correspond to pump-probe and probe-only pulses) were then spatially separated with a deviation angle of 1° 20’ using a Wollaston prism. The beams were subsequently focused to a line by a cylindrical lens (f = 25 cm) onto a 2040 x 512 16-bit CCD camera (Newton 940, Andor). This enables shot-to-shot pump-on and pump-off measurements to be made at 30 kHz. At these high lock-in rates, the excess noise, which scales as $1/v$ (where v is the measurement frequency), is very small thus improving the signal-to-noise of the difference measurement.

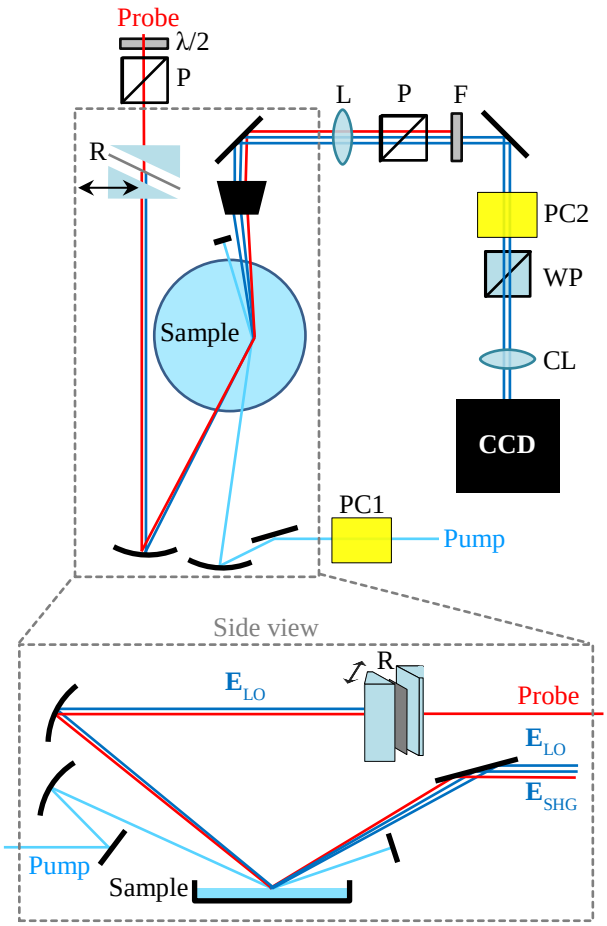

FIG 3. Schematic of the experimental set up from an above and side view. The red line indicates a path of the probe beam, the dark blue lines the second harmonic and local oscillator, and the light blue lines show the path of the pump beam. P is a polarizer, L a lens, F a filter, PC a Pockels cell, WP a Wollaston prism, CL a cylindrical lens, and R is the reference surface. The double ended arrow indicates the available translation of the second wedge used to optimise interference signals.

Experiments were performed on 50 μM aqueous solutions MG (Aldrich). The sample was contained in a standard Petri dish that was rotated (~0.5 rad s^{-1}) to continually refresh the sample. The height of the liquid surface relative to the optical table was monitored and kept constant to within ±15 μm.

IV. Results and Discussion

MG has been the subject of a number of previous investigations, including at the water/air interface using time-resolved SHG.[28,30,43] Here it is used as a proof of concept for the new experimental methodology. Figure 4 shows the relevant electronic states of MG. The excitation pulse at 257 nm is resonant with S_3 or S_4 excited states. These subsequently decay to recover the ground states. The dynamics can be tracked by probing the $S_2 \leftarrow S_0$ transition, for which the second harmonic of the 800 nm probe is resonant, resulting in resonant enhancement of the SHG field at the sample surface. Most previous experiments have used the $S_1 \leftarrow S_0$ transition, which produces a much stronger SHG response.[28,43]

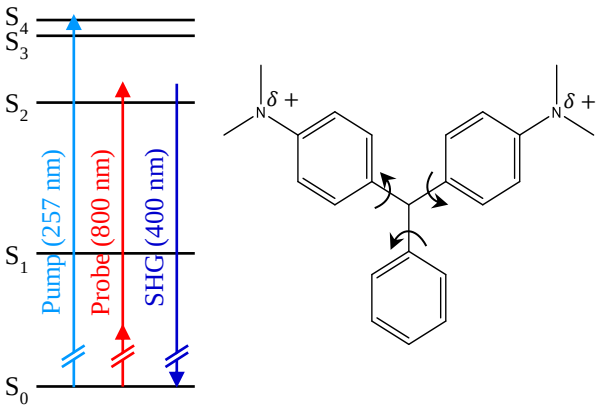

FIG 4. Schematic of the energy levels of MG (left) and its structure (right). Pump, probe and SHG energies are indicated.

Figure 5 shows that results of the experiment on MG at the water/air interface. The raw signal is shown in Figure 5(a), which shows the direct read-out from the CCD camera with a 1 s integration time. The two lines correspond to the pump-probe and probe-only signals separated by the Pockels cell and Wollaston prism combination. Superimposed on these signals are clear oscillations that corresponds to the interference fringes generated by the non-parallel pulse fronts of $\mathbf{E}_{SHG}$ and $\mathbf{E}_{LO}$. The individual lines were then integrated to provide a 1D spectrum of the profile across the pulse. This is shown in Figure 5(b) and clearly highlights the interference fringes. We note the decreasing fringe amplitude across the beam profile (towards larger pixels). This is a consequence of the reduced temporal overlap between the $\mathbf{E}_{SHG}$ and $\mathbf{E}_{LO}$ as $\mathbf{E}_{LO}$ travels through a larger portion of the wedge and thus incurs a larger group velocity delay. The current wedges have been chosen as a compromise between number of fringes (see below) and group velocity mismatch between $\mathbf{E}_{SHG}$ and $\mathbf{E}_{LO}$. The reduced interference becomes greater for shorter wavelengths. With CaF_2 wedges cut at a 10° angle, temporal overlap is maintained down to the limit of the OPA output at ~630 nm for pulses less than 230 fs. This would be further extended to shorter wavelengths by using wedges with shallower wedge angles.

Figure 5(c) shows the amplitude of the Fourier transform (defined in Eq. (1)) of both traces in (b). A peak at spatial frequency $v \sim 0.38$ rad pixel^{-1} can readily be identified both spectra and this region is expanded in Figure 5(c). At low frequency, there is a large peak (not shown here) that originates from the noise in the CCD camera and effectively has the typical $1/v$ shape of excess noise. The key benefit of measuring the interferogram is that the frequency of the interference pattern can be readily moved outside that of the noise (*i.e.* towards higher v). Hence, the Fourier transform amplitude is essentially insensitive to offsets (as exist in Figure 5b)) and small variations in the pulse profile between the two spectra.

The spatial v of the fringes is defined by the wavelength and choice of wedge angles. The wedge angle scales with v and, hence, a higher angle leads to lower noise (up to a point where $1/v$ approaches the pixel dimensions of the CCD). However, as the angle increases, so does the group velocity mismatch between $\mathbf{E}_{SHG}$ and $\mathbf{E}_{LO}$, reducing the amplitude of the Fourier transform. The compromise is one in which the signal to noise of the Fourier transform remains excellent and fringes can be seen across the profile.

The peak of the amplitude in Figure 5(c) has a shape that is determined by the amplitude variation across the pulse profile and the pulse profile itself. In principle, this allows the entire peak to be used as a measure of the amplitude. However, the phase across the peak varies significantly. In Figure 5(d), the phase as defined by Eq. (2) is shown. Note that this is a relative phase; however, it can be referenced to an absolute scale using a reference sample such a *z*-cut quartz, as we have done previously.[30] The phase varies quite erratically across the range of v where the peak in the amplitude exists. These variations arise simply because a relative phase is measured; each v would need to be calibrated to exploit the entire peak. Outside the v-range of the amplitude peak, the phases clearly do not match between the two spectra, because both real and imaginary parts are close to zero (*i.e.* there is no signal).

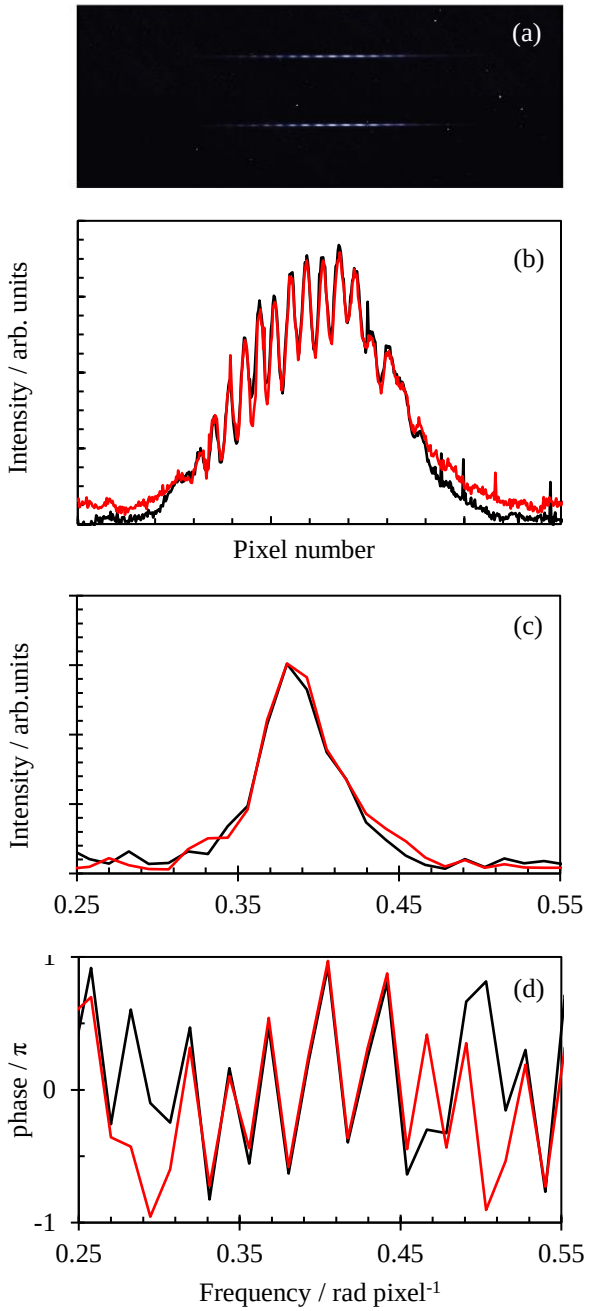

FIG 5. Results of phase sensitive SHG collected from MG at the water/air interfaces, with the pump pulse blocked. (a) The direct image output from the CCD camera with a 1 s integration time. (b) Interference pattern following the selection of a region of interest and vertical integration. (c) and (d) The amplitude and phase, respectively, recovered from Fourier transforms of each line in (b).

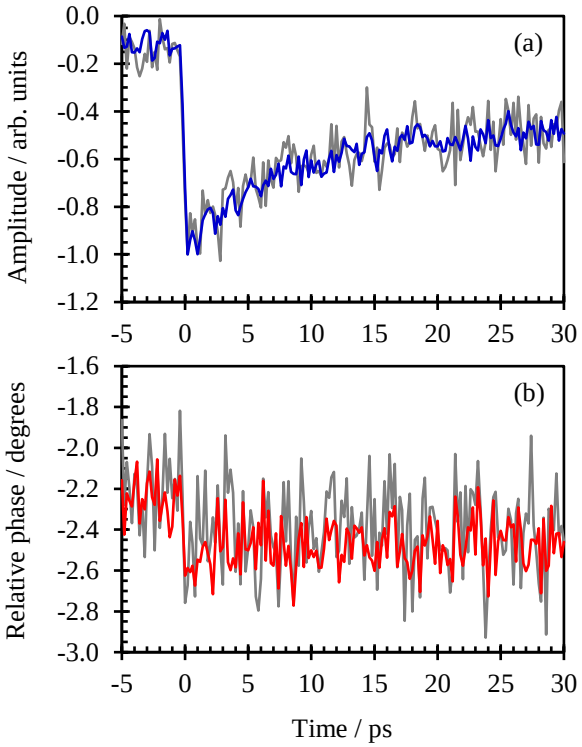

FIG 6. Time-resolved amplitude (a) and relative phase (b) of the ground state recovery of MG at the water/air interface. The coloured lines show an average of 10 measurements and the grey lines show a single measurement based on 1 s exposure times of the CCD at each time point.

Finally, we demonstrate the methodology by probing the dynamics of MG following excitation at 257 nm. Specifically, the S_0 state recovery was probed by delaying the 800 nm probe relative to the pump. In Figure 6(a), the difference in the Fourier transform amplitude is shown for pump-probe and probe-only interferograms (see Figure 5(c)) at $\nu = 0.38$ rad pixel^{-1}. For $t < 0$, the signal is close to zero. In principle, of course, it should be exactly 0, but small variations in the fringes result is a small offset. These probably arise from variations across the CCD array or imperfections in the polarisation change introduced by the ADP Pockels cell, leading to small variations between the two lines in Figure 5(a). As it is an experimental artefact, this simple offset that can be subtracted off, but we have not done so here for transparency. At $t = 0$, the signal rapidly become very negative – that is, the pump-probe amplitude (Figure 5(c)) becomes smaller than the pump-only amplitude. As the SHG at

400 nm is resonant with the $S_2 \leftarrow S_0$ transition, excitation to the S_3/S_4 result in a ground-state bleaching of the interference amplitude as less molecules are in S_0. Note that, because the signal is an interference term (see introduction), the change in signal is linearly proportional to $\mathbf{E}_{SHG}$ and therefore also N_S (the number of MG molecules in S_0 per unit area).[30]

After ~10 ps, the signal recovers and then decays further on a much longer time-scale. The initial decay can be fit to a single exponential with a lifetime of 6.7 ps. The measured lifetime is in reasonable agreement with previous work[28,43] although these experiments followed the MG dynamics by probing the $S_1 \leftarrow S_0$ transition of MG at ~620 nm. In Figure 6(b), the change in phase at $v = 0.38$ rad pixel^{-1} is shown. This is shown in degrees for clarity and, corresponds to the relative phase of pump-probe to probe-only signals. At $t = 0$, there is a clear change in phase. The phase shift amounts to 0.7 ± 0.3°, which, while very small, is perfectly reproducible. At present, we do not quite understand the origin of the phase change. It may be that the relative contributions of resonant and non-resonant parts of the second-order nonlinear susceptibility are changing, but this would then also show the decay dynamics. Alternatively, the phase may reflect the phase change of only the long-term decay component.

The grey data in both Figure 6(a) and (b) represents a single scan, where each data point (175 in total) is acquired over a 1 s integration time of the CCD camera (*i.e.* 3×10^4 pump-probe minus probe-only cycles). Hence, the entire dynamics trace shown for a single scan was acquired in ~3 minutes. The blue and red lines in Figure 6(a) and (b), respectively, are the average of 10 successive measurements (~30 minutes).

In the previous version of the experiment, we reported acquisition times for a pump-probe kinetic trace of similar quality as taking approximately 1 hr.[30] Crucially, however, that data only presented the dynamics in signal intensity (*i.e.* amplitude) at one phase delay and therefore did not distinguish between a change in SHG intensity due to a decreasing

amplitude of the interference pattern or alternatively a small phase shift with a constant amplitude. In order to obtain data that is comparable with present data, an interferogram would need to be constructed by repeating the kinetic experiment and multiple phase differences between 0 and π. With 8 phase points, this would have taken ~ 8 hrs. Additionally, because of the inaccuracies in defining the phase delay and long-term drifts, the phase-change observed here for MG was not observable. The improvement of the new method is thus clear as a full interference pattern is characterised at all time points in less time than it previously took to record one data point along the phase curve. Moreover, the sensitivity in phase changes is surprisingly good. Note, however, that the error in the absolute phase is relatively large, because this needs the be calibrated to a reference. Nevertheless, as one is mostly interested in changes in signals in time-resolved measurements, we anticipate that the presented relative phase stability will be very informative.

Despite the advantages outlined above and the relatively simple overall set-up of the experiment, there are many optical components that require careful alignment and small deviation can adversely affect the contrast of the fringes. Additionally, the inclusion of the wedges limits the ultimate time-resolution because the LO and fundamental pulses experience a delay along the pulse front; when too short, the two SHG pulses would experience a delay greater than their pulse duration and can no longer interfere. It is also noteworthy that, while the 30 kHz modulation provides enhanced signal-to-noise, our current sample rotation speed is not quite sufficient to ensure a fresh part of the surface is interrogated for each pulse pair. This can, in principle, be overcome by employing faster rotation devices or liquid jets.

Finally, we briefly compare our method to other techniques for measuring surface sensitive dynamics using second order non-linear spectroscopy.[2,4–7,34,44] A simple pump-probe scheme in which the total SHG signal, $\mathbf{E}_{SHG}^2$, is simpler and faster, but of course

suffers from the fact that it depends on N_S^n (and that it does not provide phase information). In the present experiment, the signal of the fringe pattern is $S_{fringe} = \mathbf{E}_{SHG}^2 + \mathbf{E}_{LO}^2 + 2\mathbf{E}_{SHG}\mathbf{E}_{LO}\sin(\phi)$, where the Fourier transform effectively recovers the term proportional to $\mathbf{E}_{SHG}\mathbf{E}_{LO}$. Hence, for a weak $\mathbf{E}_{SHG}$ response, the measured signal amplitude can be increased by increasing $\mathbf{E}_{LO}$. In reality of course, there is a limit to which point $\mathbf{E}_{LO}$ can be increased. Specifically, If $\mathbf{E}_{LO} >> \mathbf{E}_{SHG}$, then $S_{fringe} \sim \mathbf{E}_{LO}^2$ and the oscillation of amplitude $2\mathbf{E}_{SHG}\mathbf{E}_{LO}\sin(\phi)$ may not be distinguishable from the pulse profile. Therefore, the choice of reference material can become important.

In recent years, heterodyne-detected techniques have been actively developed.[32,45–50] A key advantage of these is that they also acquire spectral information which has been very informative in vibrational SFG spectroscopy.[19,47,49,50] In heterodyne-detected SFG experiments, a temporally delayed phase-locked LO is interfered with the signal and dispersed onto a CCD and the interference is measured in the frequency domain. The signal is then inverse Fourier transformed to the time domain, filtered and Fourier transformed back to obtain the imaginary and real components of the non-linear susceptibility at all measured frequencies. Often, a key challenge with such experiments is phase stability: micrometre accuracy is essential in the beams' propagation distances between the sample and reference surfaces,[30,50] although this requirement can be alleviated by reducing the angle between two non-collinear pump beams.[51] While other key advancements have been made to improve heterodyne-detected SFG set-ups,[52] our method is effectively indefinitely phase-stable as all beams are colinear and the sensitivity to phase changes is outstanding. Additionally, the shortened acquisition time for our new time-resolved measurements compares extremely favourably with the ~50 min/delay for a heterodyne-detected measurement,[50] but of course we note that this is at the expense of obtaining the full spectral information. The simplest way to gain the spectral information in the present experiment is to scan the probe photon energy.

This would in fact be quite feasible over limited ranges of ~1000 cm^{-1} in the fundamental. Beyond this, changes in alignment may be required. We note however, that most heterodyne-detected experiments are limited to smaller bandwidths.[50,53]

V. Conclusions

This paper presents a new time-resolved technique for studying dynamics at the interface between bulk centrosymmetric media. In essence the technique is an improvement to phase-sensitive SHG measurements that measures the interference between sample generated SHG field and a local oscillator SHG field (LO) from a reference.[30] By using a spatially varying phase unit, comprised of two wedges between which the reference surface is positioned, combined with a 30 kHz lock-in measurement, pump-probe measurements can be recorded with extraordinary sensitivity to phase changes. The applicability is demonstrated on the dynamics of malachite green at the water/air interface, for which we show that excellent time-resolved amplitude and phase information can be obtained in short data acquisition times.

Acknowledgements

We are grateful to Kelvin Appleby for constructing the driving electronics for the Pockels cells and Paweł Nowakowski for assistance in the early stages of the experiment. This work was funded by the European Research Council (306536). A. L. Tyson was supported by the Durham Doctoral Scholarship scheme.

References

[1] Y.R. Shen, Nature **337**, 519 (1989).

[2] K.B. Eisenthal, Chem. Rev. **96**, 1343 (1996).

[3] G.L. Richmond, Chem. Rev. **102**, 2693 (2002).

[4] F.M. Geiger, Annu. Rev. Phys. Chem. **60**, 61 (2009).

[5] Y.R. Shen, Annu. Rev. Phys. Chem. **64**, 129 (2013).

[6] S. Nihonyanagi, S. Yamaguchi, and T. Tahara, Chem. Rev. **117**, 10665 (2017).

[7] R.M. Corn and D.A. Higgins, Chem. Rev. **94**, 107 (1994).

[8] P. Guyot-Sionnest, J.H. Hunt, and Y.R. Shen, Phys. Rev. Lett. **59**, 1597 (1987).

[9] J.H. Hunt, P. Guyot-Sionnest, and Y.R. Shen, Chem. Phys. Lett. **133**, 189 (1987).

[10] L.J. Richter, T.P. Petralli-Mallow, and J.C. Stephenson, Opt. Lett. **23**, 1594 (1998).

[11] J.A. McGuire, W. Beck, X. Wei, and Y.R. Shen, Opt. Lett. **24**, 1877 (1999).

[12] R.K. Chang, J. Ducuing, and N. Bloembergen, Phys. Rev. Lett. **15**, 6 (1965).

[13] K. Kemnitz, K. Bhattacharyya, J.M. Hicks, G.R. Pinto, B. Eisenthal, and T.F. Heinz, Chem. Phys. Lett. **131**, 285 (1986).

[14] T.F. Heinz, H.W.K. Tom, and Y.R. Shen, Phys. Rev. A **28**, 1883 (1983).

[15] H.W.K. Tom, T.F. Heinz, and Y.R. Shen, Phys. Rev. Lett. **51**, 1983 (1983).

[16] R. Superfine, J.Y. Huang, and Y.R. Shen, Opt. Lett. **15**, 1276 (1990).

[17] N. Ji, V. Ostroverkhov, C.-Y. Chen, and Y.-R. Shen, J. Am. Chem. Soc. **129**, 10056 (2007).

[18] W. Gan, D. Wu, Z. Zhang, R. Feng, and H. Wang, J. Chem. Phys. **124**, 114705 (2006).

[19] S. Nihonyanagi, S. Yamaguchi, and T. Tahara, J. Chem. Phys. **130**, 204704 (2009).

[20] X. Chen, W. Hua, Z. Huang, and H.C. Allen, J. Am. Chem. Soc. **132**, 11336 (2010).

[21] J.A. McGuire and Y.R. Shen, Science **313**, 1945 (2006).

[22] X. Wei and Y.R. Shen, Phys. Rev. Lett. **86**, 4799 (2001).

[23] H. Arnolds and M. Bonn, Surf. Sci. Rep. **65**, 45 (2010).

[24] D. Zimdars, J.I. Dadap, K.B. Eisenthal, and T.F. Heinz, J. Phys. Chem. B **103**, 3425 (1999).

[25] A. Castro, E.V. Sitzmann, D. Zhang, and K.B. Eisenthal, J. Phys. Chem. **95**, 6752 (1991).

[26] R. Antoine, A.A. Tamburello-Luca, P. Hébert, P.F. Brevet, and H.H. Girault, Chem. Phys. Lett. **288**, 138 (1998).

[27] J. Sung and D. Kim, J. Phys. Chem. C **111**, 1783 (2007).

[28] X. Shi, E. Borguet, A.N. Tarnovsky, and K.B. Eisenthal, Chem. Phys. **205**, 167 (1996).

[29] D.M. Sagar, C.D. Bain, and J.R.R. Verlet, J. Am. Chem. Soc. **132**, 6917 (n.d.).

[30] P.J. Nowakowski, D.A. Woods, C.D. Bain, and J.R.R. Verlet, J. Chem. Phys. **142**, 084201 (2015).

[31] G. Lüpke, G. Marowsky, and R. Steinhoff, Appl. Phys. B **49**, 283 (1989).

[32] I.V. Stiopkin, H.D. Jayathilake, A.N. Bordenyuk, and A.V. Benderskii, J. Am. Chem. Soc. **130**, 2271 (2008).

[33] P.J. Nowakowski, D.A. Woods, and J.R.R. Verlet, J. Phys. Chem. Lett. **7**, 4079 (2016).

[34] R. Stolle, G. Marowsky, E. Schwarzberg, and G. Berkovic, Appl. Phys. B **63**, 491 (1996).

[35] F. Kanal, S. Keiber, R. Eck, and T. Brixner, Opt. Express **22**, 16965 (2014).

[36] F. Preda, V. Kumar, F. Crisafi, D.G.F. del Valle, G. Cerullo, and D. Polli, Opt. Lett. **41**, 2970 (2016).

[37] B.I. Greene, R.M. Hochstrasser, and R.B. Weisman, J. Chem. Phys. **70**, 1247 (1979).

[38] C.C. Gradinaru, J.T.M. Kennis, E. Papagiannakis, I.H.M. van Stokkum, R.J. Cogdell, G.R. Fleming, R.A. Niederman, and R. van Grondelle, Proc. Natl. Acad. Sci. **98**, 2364 (2001).

[39] S.A. Kovalenko, N.P. Ernsting, and J. Ruthmann, Chem. Phys. Lett. **258**, 445 (1996).

[40] A.C. Bhasikuttan, A.V. Sapre, and T. Okada, J. Phys. Chem. A **107**, 3030 (2003).

[41] D.J. Erskine, A.J. Taylor, and C.L. Tang, J. Chem. Phys. **80**, 5338 (1984).

[42] J. Mishra, P.K. Mishra, and P.K. Khare, in *AIP Conf. Proc.* (AIP Publishing, 2011), pp. 561–562.

[43] A. Punzi, G. Martin-Gassin, J. Grilj, and E. Vauthey, J. Phys. Chem. C **113**, 11822 (2009).

[44] P.L. Geissler, Annu. Rev. Phys. Chem. **64**, 317 (2013).

[45] M.S. Fee, K. Danzmann, and S. Chu, Phys. Rev. A **45**, 4911 (1992).

[46] K. Inoue, S. Nihonyanagi, P.C. Singh, S. Yamaguchi, and T. Tahara, J. Chem. Phys. **142**, 212431 (2015).

[47] P. Mathi, B.N. Jagatap, and J.A. Mondal, J. Phys. Chem. C **121**, 7993 (2017).

[48] K. Matsuzaki, R. Kusaka, S. Nihonyanagi, S. Yamaguchi, T. Nagata, and T. Tahara, J. Am. Chem. Soc. **138**, 7551 (2016).

[49] J.A. Mondal, S. Nihonyanagi, S. Yamaguchi, and T. Tahara, J. Am. Chem. Soc. **132**, 10656 (2010).

[50] S. Nihonyanagi, J.A. Mondal, S. Yamaguchi, and T. Tahara, Annu. Rev. Phys. Chem. **64**, 579 (2013).

[51] P.A. Covert, W.R. FitzGerald, and D.K. Hore, J. Chem. Phys. **137**, 014201 (2012).

[52] H. Vanselous and P.B. Petersen, J. Phys. Chem. C **120**, 8175 (2016).

[53] I.V. Stiopkin, H.D. Jayathilake, C. Weeraman, and A.V. Benderskii, J. Chem. Phys. **132**, 234503 (2010).